

**Isolated and modulated effects of topology and material type on the mechanical properties of additively manufactured porous biomaterials**

Hedayati, R.; Ahmadi, S. M.; Lietaert, K.; Pouran, B.; Li, Y.; Weinans, H.; Rans, C. D.; Zadpoor, A. A.

**DOI**

[10.1016/j.jmbbm.2017.12.029](https://doi.org/10.1016/j.jmbbm.2017.12.029)

**Publication date**

2018

**Document Version**

Final published version

**Published in**

Journal of the Mechanical Behavior of Biomedical Materials

**Citation (APA)**

Hedayati, R., Ahmadi, S. M., Lietaert, K., Pouran, B., Li, Y., Weinans, H., Rans, C. D., & Zadpoor, A. A. (2018). Isolated and modulated effects of topology and material type on the mechanical properties of additively manufactured porous biomaterials. *Journal of the Mechanical Behavior of Biomedical Materials*, 79, 254-263. <https://doi.org/10.1016/j.jmbbm.2017.12.029>

**Important note**

To cite this publication, please use the final published version (if applicable). Please check the document version above.

**Copyright**

Other than for strictly personal use, it is not permitted to download, forward or distribute the text or part of it, without the consent of the author(s) and/or copyright holder(s), unless the work is under an open content license such as Creative Commons.

**Takedown policy**

Please contact us and provide details if you believe this document breaches copyrights. We will remove access to the work immediately and investigate your claim.



Contents lists available at ScienceDirect

# Journal of the Mechanical Behavior of Biomedical Materials

journal homepage: [www.elsevier.com/locate/jmbbm](http://www.elsevier.com/locate/jmbbm)

## Isolated and modulated effects of topology and material type on the mechanical properties of additively manufactured porous biomaterials

R. Hedayati<sup>a,b,1,\*</sup>, S.M. Ahmadi<sup>a,1</sup>, K. Lietaert<sup>c</sup>, B. Pouran<sup>a,b</sup>, Y. Li<sup>a</sup>, H. Weinans<sup>a,b,d</sup>, C.D. Rans<sup>e</sup>, A.A. Zadpoor<sup>a</sup>

<sup>a</sup> Department of Biomechanical Engineering, Faculty of Mechanical, Maritime, and Materials Engineering, Delft University of Technology (TU Delft), Mekelweg 2, 2628 CD, Delft, The Netherlands

<sup>b</sup> Department of Orthopedics, University Medical Center Utrecht, Heidelberglaan100, 3584CX Utrecht, The Netherlands

<sup>c</sup> 3D Systems – LayerWise NV, Grauwmeer 14, 3001 Leuven, Belgium

<sup>d</sup> Department of Rheumatology, University Medical Center Utrecht, Heidelberglaan100, 3584CX Utrecht, The Netherlands

<sup>e</sup> Faculty of Aerospace Engineering, Delft University of Technology, 2629 HS Delft, The Netherlands

### ARTICLE INFO

#### Keywords:

Microstructure  
porous biomaterial  
additive manufacturing  
selective laser melting

### ABSTRACT

In this study, we tried to quantify the isolated and modulated effects of topological design and material type on the mechanical properties of AM porous biomaterials. Towards this aim, we assembled a large dataset comprising the mechanical properties of AM porous biomaterials with different topological designs (i.e. different unit cell types and relative densities) and material types. Porous structures were additively manufactured from Co-Cr using a selective laser melting (SLM) machine and tested under quasi-static compression. The normalized mechanical properties obtained from those structures were compared with mechanical properties available from our previous studies for porous structures made from Ti-6Al-4V and pure titanium as well as with analytical solutions. The normalized values of elastic modulus and yield stress were found to be relatively close to each other as well as in agreement with analytical solutions regardless of material type. However, the material type was found to systematically affect the mechanical properties of AM porous biomaterials in general and the post-elastic/post-yield range (plateau stress and energy absorption capacity) in particular. To put this in perspective, topological design could cause up to 10-fold difference in the mechanical properties of AM porous biomaterials while up to 2-fold difference was observed as a consequence of changing the material type.

### 1. Introduction

Recent advances in additive manufacturing (AM) techniques have enabled fabrication of porous biomaterials with arbitrarily complex topology of the micro-architecture. Since the mechanical properties of such AM porous biomaterials are directly related to the topology of their microarchitecture (Lin et al., 2004; Hollister et al., 2002; Hollister, 2005; Bandyopadhyay and Bose, 2016; Bandyopadhyay et al., 2010; Krishna et al., 2008), it is possible to design porous biomaterials that satisfy certain design objectives. For example, AM porous biomaterials with mechanical properties similar to those of native bone tissue could be made from metallic alloys whose mechanical properties are a few orders of magnitude higher than bone (Staiger et al., 2006; Krishna et al., 2007; Bandyopadhyay et al., 2009). This decreased stiffness prevents a common problem associated with solid implants known as

stress shielding. The open-cell interconnected hollow space inside porous implants also allows for adjustment of scaffold permeability (Van Bael et al., 2012; Zadpoor, 2015) to facilitate mass transport and, thus, cell oxygenation and nutrition. Moreover, bone could grow into the open pore structure, which in turn results in improved implant fixation and osseointegration (Hutmacher, 2000; Liu et al., 2011). Finally, the porous structure increases the surface area of such AM biomaterials, which could then be used for bio-functionalization purposes, for example, to attach molecules that improve bone tissue regeneration performance (Pattanayak et al., 2011; Pyka et al., 2012; Yavari et al., 2014) or to induce antibacterial effects (Vaithilingam et al., 2014; Jia et al., 2016; Amin Yavari et al., 2016).

Most of the properties discussed above including the mechanical properties, mass transport properties (such as permeability), and surface area are directly related to the topology of the micro-architecture

\* Corresponding author at: Department of Biomechanical Engineering, Faculty of Mechanical, Maritime, and Materials Engineering, Delft University of Technology (TU Delft), Mekelweg 2, 2628 CD, Delft, The Netherlands.

E-mail addresses: [r.hedayati@tudelft.nl](mailto:r.hedayati@tudelft.nl), [rezahedayati@gmail.com](mailto:rezahedayati@gmail.com) (R. Hedayati).

<sup>1</sup> Both authors equally contributed to this work.

of additively manufactured porous biomaterials. That is why a major paradigm in the development of such biomaterials has been “topological design” (Wang et al., 2016). Within the context of mechanical properties, topological design refers to the adjustment of the quasi-static (Amin Yavari et al., 2015; Ptochos and Labeas, 2012; Han et al., 2017) and fatigue (Van Hooreweder et al., 2017; Hedayati et al., 2016) properties of additively manufactured porous biomaterials through rational design of the geometry of their micro-architecture. This approach has been supported by a relatively large number of studies within the last few years that have found that the normalized (i.e. the ratio of a property in the porous structure to that of the bulk material) elastic mechanical properties including the elastic modulus, yield stress, and Poisson’s ratio of AM porous biomaterials are strongly dependent on the topology of the porous structure (Hedayati et al., 2016; Hedayati et al., 2016; Babaee et al., 2012; Zheng et al., 2014; Warren and Kraynik, 1997). The relevant topological parameters include relative density or adjustable porosity, geometry of the strut cross-section, and shape of the unit cell (Hedayati et al., 2016a, 2016b; Babaee et al., 2012; Zheng et al., 2014; Warren and Kraynik, 1997; Li et al., 2014; Ko, 1965; Zhu et al., 1997).

Given the direct and strong influence of topology, the vast majority, if not all, of analytical and computational models used for predicting the mechanical properties of such biomaterials assume that the *normalized* mechanical properties of AM porous biomaterials are the same regardless of the material used for making the porous structure (Babaee et al., 2012; Gibson and Ashby, 1999; Ahmadi et al., 2014). In other words, previous studies have assumed there is no modulation between the material type and topology in determining the mechanical properties of AM porous biomaterials. Therefore, the material properties of the bulk material can be used as scale factors which convert the normalized mechanical properties of the porous structure to its absolute values.

In this study, we aim to determine whether such an assumption is valid and, thus, try to separate the effects of topology from those of material type. Investigating the effects of material type is important, because laser processing parameters and the resulting microstructure as well as bulk material properties could change from one material to the other. A large dataset of the mechanical properties of AM porous biomaterials based on various types of topological designs and different material types is needed to answer the above-mentioned research question. We therefore used selective laser melting to manufacture porous metallic biomaterials from Co-Cr with three different types of repeating unit cells and three to four porosities (for each unit cell type). The topological features and compressive mechanical properties of the obtained specimens were then determined respectively using micro-computed tomography ( $\mu$ CT) and mechanical testing. In our previous studies, we had additively manufactured, topologically characterized, and mechanically tested similar (same unit cell designs) porous structures from two other material types titanium alloy Ti-6Al-4V (Ahmadi et al., 2015) and pure titanium (Wauthle et al., 2015). The entire dataset of three different types of materials, three types of repeating unit cells, and multiple porosities was then used to determine whether or not there is a modulation between the material type and topology in determining the *normalized* mechanical properties of AM porous biomaterials.

## 2. Materials and methods

### 2.1. Materials and manufacturing

Co-Cr porous structures (Fig. 1) were additively manufactured using a ProX DMP 320 3D printer (3D Systems, SC, United States). Co-Cr powder (Cr 28.5%, Mo 6%, other specifications according to ASTM F75) was processed on top of a solid substrate under an inert atmosphere with less than 50 ppm of O<sub>2</sub>. Three different unit cell types (truncated cuboctahedron, diamond, and rhombic dodecahedron) were chosen for fabricating the porous structures. For each unit cell type,

different strut thicknesses were used in order to achieve porous structures with different relative densities (Table 1). All specimens were cylindrical in shape with diameters of 15 mm and lengths of 20 mm. The unit cell size was 1.5 mm. In addition to porous biomaterials, several solid specimens were additively manufactured and tested to obtain the mechanical properties of the bulk material (Fig. 2 and Table 2). For the bulk Co-Cr material, the elastic modulus was obtained using an MTS with 500 kN load cell (MTS Systems Corporation, Eden Prairie, MN, USA) mechanical testing machine and a setup employing the impulse excitation technique (RFDA basic, IMCE, Genk, Belgium) that works on the basis of measuring natural frequencies in vibration (Heritage et al., 1988). Several solid cylindrical samples with diameters of 15 mm and lengths of 20 mm were additively manufactured and compressed with displacement rate of 1.8 mm/min. To leave out the non-sample displacement from the results read from the test machine, the load-displacement of the machine without installed sample was obtained and subtracted from the results (Kalidindi et al., 1997). As another displacement recording method, KFG-5-120-D16-11 (KYOWA, Japan) strain gauges (length of 5 mm, resistance of  $119.8 \pm 0.3 \Omega$ , adoptable thermal expansion of 11.7 PPM/°C) were installed on the solid cylindrical samples. The specimens used for impulse excitation technique were brick-shaped with the following dimensions:  $6.9 \times 34.9 \times 89.5 \text{ mm}^3$ . The stress-strain curves and mechanical properties of the porous structures with the same unit cell types but made from Ti-6Al-4V (Ahmadi et al., 2015) and pure titanium (Wauthle et al., 2015) were adopted from our previous studies and were used for comparison purposes.

### 2.2. Topological characterization

Dry weighing and  $\mu$ CT scanning were both used to determine the relative density of the porous structures. In dry weighing, the weight of each specimen was measured in room temperature and in normal atmospheric conditions. The measured weight was then divided by the volume of the specimens to determine the density of the specimens. The obtained density of the specimens was then divided by the density of the bulk material they were made of (i.e.  $8800 \text{ kg/m}^3$ ) to obtain the relative density of the porous structures.

In another approach, the Co-Cr porous structures were imaged using a  $\mu$ CT scanner (Quantum FX, Perkin Elmer, USA) (Fig. 3). Pure titanium (Wauthle et al., 2015) and Ti-6Al-4V (Ahmadi et al., 2015) structures were also imaged using the same scanner. The porous structures were scanned under a tube current of 180  $\mu$ A and a tube voltage of 90 kV. The scan time was 3 min and the voxel size of the images was  $42 \mu\text{m} \times 42 \mu\text{m} \times 42 \mu\text{m}$ . The automatically reconstructed  $\mu$ CT images were converted into a series of 2D images using Analyze 11.0 (Perkin Elmer, USA). The 2D images were exported to Fiji (NIH, Bethesda, MD, USA) and regions of interest (ROIs) were defined. After local segmentation in Fiji, the prebuilt plugin of BoneJ (available in ImageJ) was used to calculate the ratio of void volume to the 3D ROI volume, the strut size as well as the pore size of the scaffolds.

### 2.3. Microstructural analysis

For each series of porous structures, one sample was chosen for micro-structural observation. Specimens were first ground from 80 to 2000 grit size and then polished respectively with 3  $\mu\text{m}$  and 1  $\mu\text{m}$  polishing papers. Different etching solutions were used to reveal the grains of Co-Cr porous structures mechanically tested here as well as pure titanium and Ti-6Al-4V specimens used in our previous studies. Pure titanium and Ti-6Al-4V samples were immersed in the Keller’s etchant (190 ml water + 5 ml nitric acid + 3 ml Hydrochloric acid + 2 ml Hydrofluoric acid) for about 150 s. Co-Cr samples were immersed in a solution of 37% HCl + 1 g K<sub>2</sub>S<sub>2</sub>O<sub>5</sub> for about 5 min. The micro-structure of the specimens was observed with an optical microscope (OM, model BX60M, Olympus) and a scanning electron microscope

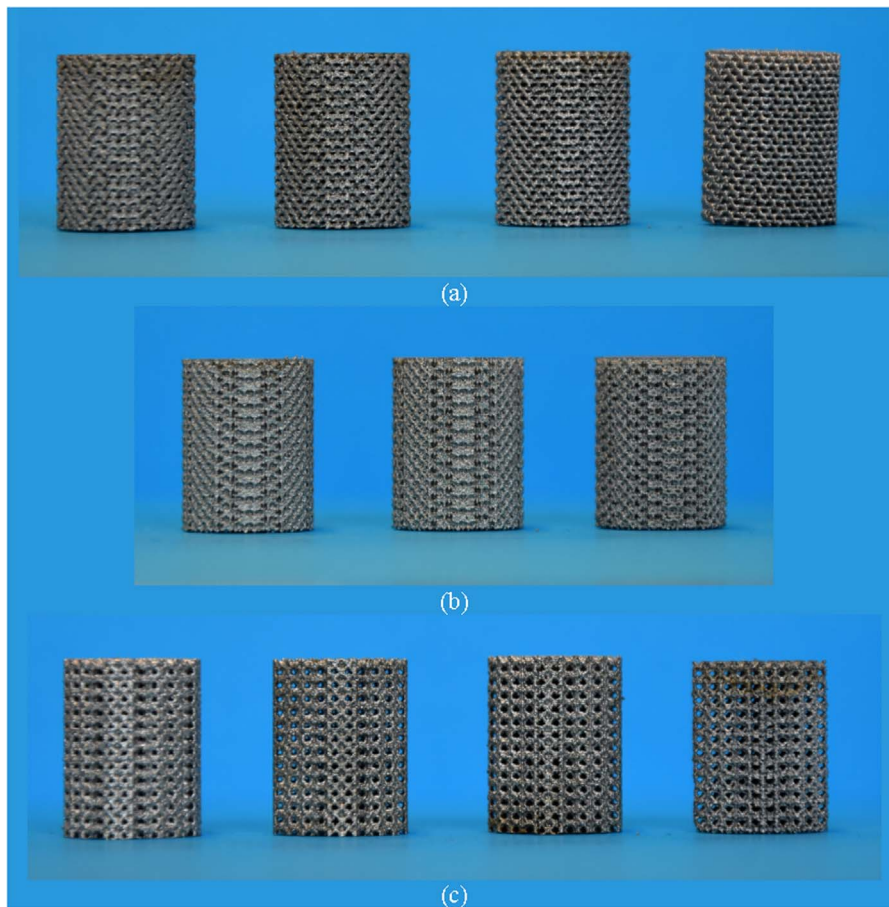


Fig. 1. - Side view of the additively manufactured Co-Cr porous structures based on (a) diamond (b) rhombic dodecahedron, and (c) truncated cuboctahedron unit cells.

**Table 1**  
Topological design and morphological properties of the porous structures having different unit cell types and sizes.

	Relative density		Strut size ( $\mu\text{m}$ )		Pore size ( $\mu\text{m}$ )	
	Dry weighting ( $\pm$ SD)	$\mu\text{CT}$ ( $\pm$ SD)	Nominal (Design)	$\mu\text{CT}$ ( $\pm$ SD)	Nominal (Design)	$\mu\text{CT}$ ( $\pm$ SD)
<b>Truncated cuboctahedron (TCO)</b>						
TCO-1	$0.24 \pm 0.003$	$0.27 \pm 0.005$	324	$343.20 \pm 102.7$	876	$917.76 \pm 334.6$
TCO-2	$0.27 \pm 0.07$	$0.28 \pm 0.01$	356	$339.84 \pm 101.3$	844	$895.20 \pm 325.4$
TCO-3	$0.34 \pm 0.002$	$0.33 \pm 0.004$	410	$396.96 \pm 125.3$	790	$821.47 \pm 323.8$
TCO-4	$0.39 \pm 0.007$	$0.42 \pm 0.01$	460	$433.58 \pm 146.9$	740	$669.31 \pm 293.1$
<b>Rhombic dodecahedron (RD)</b>						
RD-1	$0.30 \pm 0.002$	$0.29 \pm 0.005$	310	$349.44 \pm 103.15$	590	$506.26 \pm 167.4$
RD-2	$0.37 \pm 0.002$	$0.47 \pm 0.006$	370	$402.53 \pm 127.3$	530	$492.58 \pm 185.1$
RD-3	$0.41 \pm 0.002$	$0.53 \pm 0.005$	430	$446.40 \pm 160.95$	470	$431.76 \pm 171.4$
<b>Diamond (D)</b>						
D-1	$0.21 \pm 0.001$	$0.27 \pm 0.005$	320	$357.22 \pm 62.2$	580	$650.74 \pm 116.3$
D-1	$0.27 \pm 0.002$	$0.3 \pm 0.004$	375	$390.38 \pm 85.8$	525	$541.49 \pm 127$
D-3	$0.34 \pm 0.003$	$0.44 \pm 0.009$	415	$440.93 \pm 109.6$	485	$465.60 \pm 125.5$
D-4	$0.40 \pm 0.001$	$0.53 \pm 0.005$	450	$486.29 \pm 145$	450	$411.36 \pm 131.2$

(SEM, JSM-IT100, JEOL).

#### 2.4. Static mechanical testing

The mechanical tests were carried out using an Instron 5985 mechanical testing machine with a 100 kN load cell. The loading rate was set to 1.8 mm/min. The methodology used for carrying out the experimental tests was the same as the one described in the ISO standard 13314:2011 (ISO Standard, 2011) which specifies the compression test methods for porous and cellular metals. The porous structures based on the diamond and truncated cuboctahedron unit cells were compressed

up to 60% strain, while the porous structures based on the rhombic dodecahedron unit cell were compressed up to 80% strain. The mechanical tests were repeated three times for each type of porous structure. The mechanical properties obtained from three samples of each type were used to calculate the mean and standard deviations of the corresponding mechanical properties. The following mechanical properties were calculated: elastic modulus, yield stress, plateau stress, and energy absorption. Elastic modulus was determined by measuring the slope of the initial linear part of the stress-strain curve. Yield stress was obtained by offsetting a line to the right side of the initial linear part of the stress-strain curve for 0.2 % strain and obtaining its

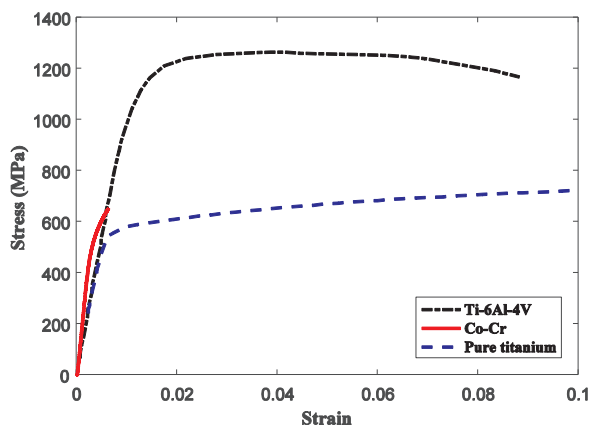


Fig. 2. Stress-strain curves of different bulk materials used for additive manufacturing of porous biomaterials.

Table 2  
Mechanical properties of the bulk materials.

	$\sigma_{ys}$ [MPa]	$E_s$ [GPa]
Ti-6Al-4V (Ahmadi et al., 2014)	980	122
Co-Cr	657	201.5 (Mechanical test) 205 (Impulse Excitation)
Commercial pure titanium (CPT) (Wauthle et al., 2015)	300	100

intersection with the stress-strain curve. Plateau stress refers to the second stage of the stress-strain curves in which the strain value increases significantly with minor change in stress value. As suggested by the ISO standard 13314:2011 (ISO Standard, 2011), to calculate the plateau stress, the arithmetical mean of stresses values between 20% and 40% strains were determined. The energy absorption capacity of each structure was defined as the area below the load-displacement curve for up to 50% strain.

The noted parameters were plotted against the relative density of the porous structures as determined by dry weighing. To be able to compare the mechanical properties of porous structures systematically, power law relationships, i.e.  $P = a\mu^b$ , where  $P$  stands for the property and  $\mu$  represents the relative density of the porous structure, were fitted to all the mechanical property-relative density data points. The constants  $a$  and  $b$  are reported in the corresponding curves.

To measure the hardness of the struts, the cross-section of each specimen was grinded to 320 grit size and then polished to 9  $\mu\text{m}$  (diamond suspension). The HV 0.5 test protocol devised for measuring the Vickers hardness (DuraScan-70, Struers, Netherlands) was used. The loading time was set to 10 s. The hardness was measured in 20 random

positions on the cross-section of the porous structures, and their average value as well as the standard deviation was calculated.

To compare the experimental elastic modulus and yield stress curves with the analytical values, analytical relationships presented in (Babae et al., 2012; Ahmadi et al., 2014; Hedayati et al., 2016) will be used

### 3. Results

The Vicker’s micro-hardness measurements on porous structures gave the hardness values of  $461 \pm 30$ ,  $433 \pm 9$ , and  $220 \pm 18$  for the Co-Cr, Ti-6Al-4V, and pure titanium structures, respectively. The typical optical microscopy images of the cross-section of three sample specimens are presented in Figure S1. Pure titanium showed lath-shaped grains with a length range of sizes between 20 and 50  $\mu\text{m}$ , which could be identified as a hexagonal close packing (hcp)  $\alpha$  phase (Figure S1a). A fully acicular  $\alpha'$  martensitic microstructure was developed in Ti-6Al-4V during the SLM process, which had lengths in the range of 10-20  $\mu\text{m}$  (Figure S1b) and widths in the range of 1-2  $\mu\text{m}$  (Figure S2a). The grains of Co-Cr material were of elongated cellular shape with diameters around 1  $\mu\text{m}$  (Figure S1d and Figure S2b). The welding lines between different melting pools of Co-Cr porous structures were visible in the microstructural images (Figure S1c). The grain growth direction was different for different melt pools (Figure S1d).

Under compression, all the structures demonstrated the three-stage stress-strain curves that are typical of porous structures including porous biomaterials ( Figs. 4–6). The first part was linear elastic after which the slope of the diagram rapidly decreased. In the second stage (known as the plateau stage), the strain increased significantly with small increases in the stress value. In the final stage known as the densification stage, the stress started to increase exponentially (Figs. 4–6). For all the relative densities of the porous structures based on the diamond unit cell, densification occurred in strains about 40% (Fig. 4). In the porous structures based on the rhombic dodecahedron and truncated octahedron unit cells, densification occurred at strains around 60%. In high-density ( $\mu = 0.415$ ) porous structures based on the rhombic dodecahedron unit cell, densification started earlier ( $\epsilon_d \approx 41.5\%$ ) (Fig. 5c).

Using the stress-strain curves obtained from different specimens, the normalized elastic modulus, yield stress, plateau stress, and energy absorption of all the specimens were determined and plotted against relative density (Figs. 7–10). In two of the graphs (i.e. normalized elastic modulus and normalized yield stress) for which analytical relationships were available from the literature (Babae et al., 2012; Ahmadi et al., 2014; Hedayati et al., 2016), analytical curves are plotted as well (Figs. 7 and 8).

Regardless of the unit cell type, the normalized values of the elastic moduli and yield stress for the porous structures made from both Ti-6Al-4V and Co-Cr were in general agreement with each other (Figs. 7 and 8). As for the normalized plateau stress diagrams, the results of both Co-Cr and Ti-6Al-4V structures were close to each other for

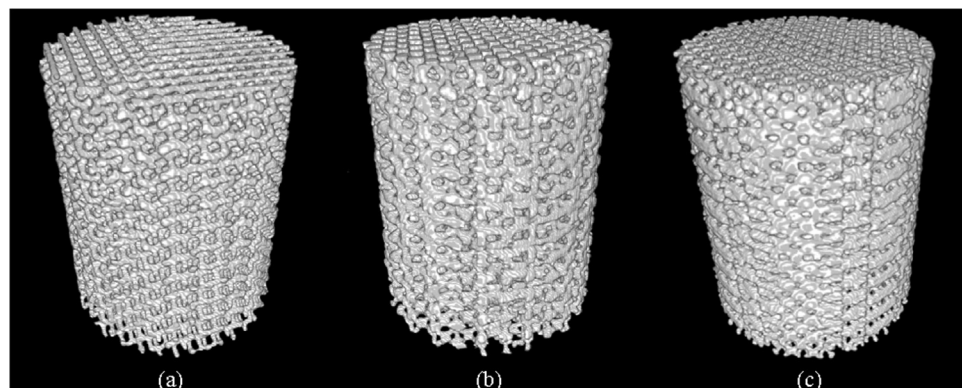


Fig. 3. Reconstructed CT images of Co-Cr porous structures based on (a) diamond, (b) truncated cuboctahedron, and (c) rhombic dodecahedron unit cells.

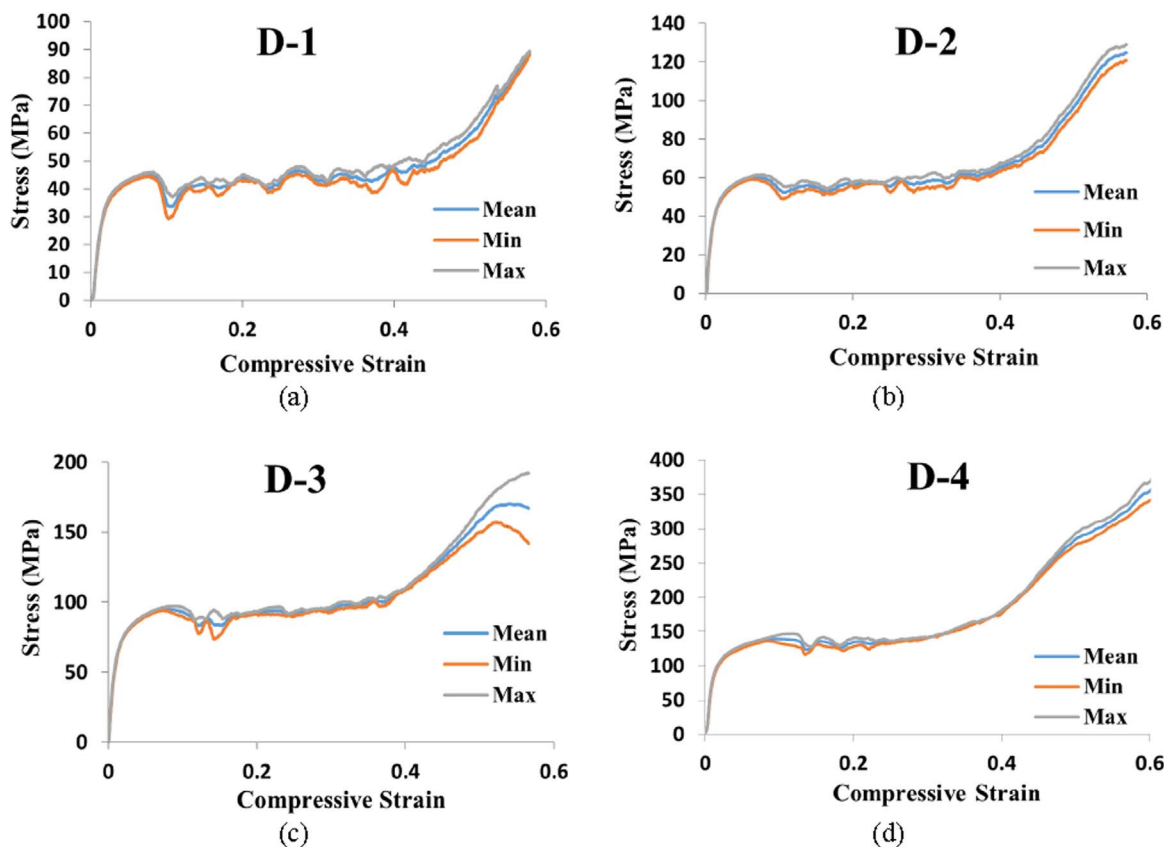


Fig. 4. Stress-strain curves of Co-Cr porous structures based on diamond unit cell with different relative density values: (a) 0.21, (b) 0.27, (c) 0.34, and (d) 0.40.

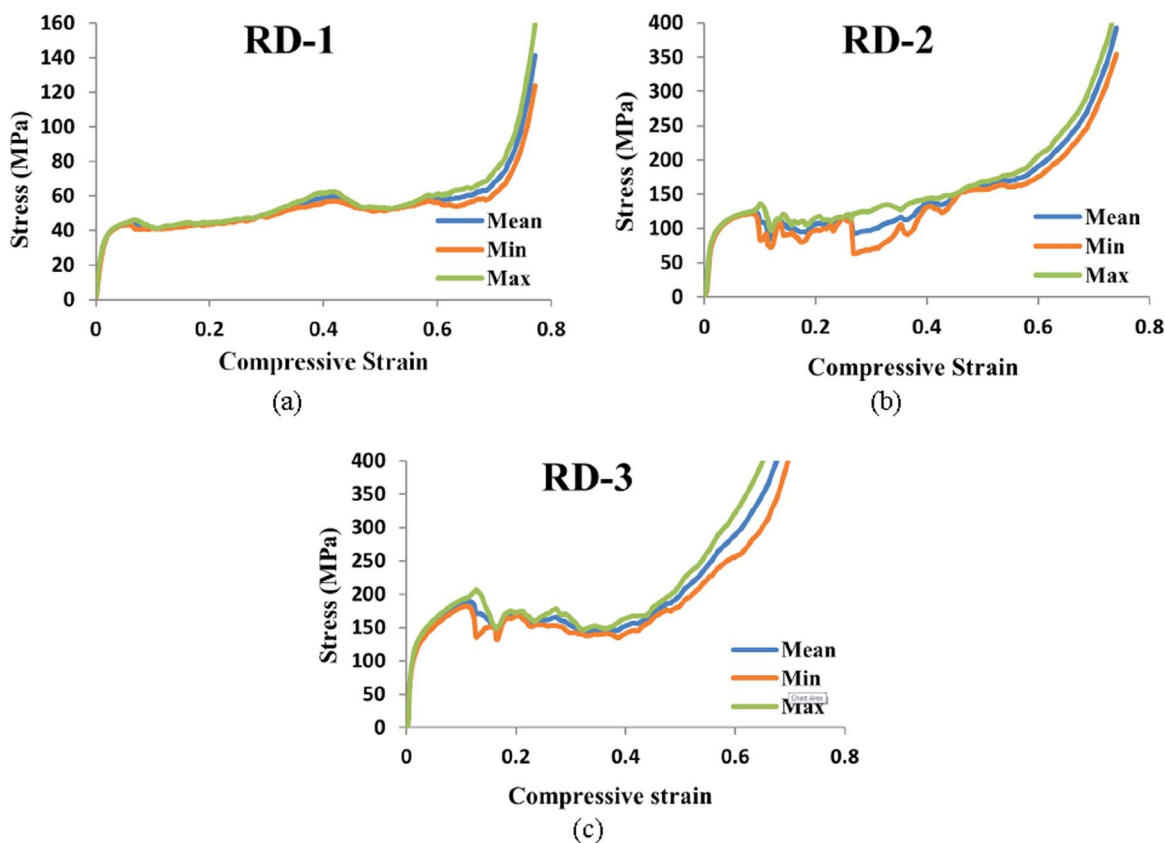


Fig. 5. Stress-strain curves of Co-Cr porous structures based on rhombic dodecahedron unit cell with different relative density values: (a) 0.30, (b) 0.37, and (c) 0.41.

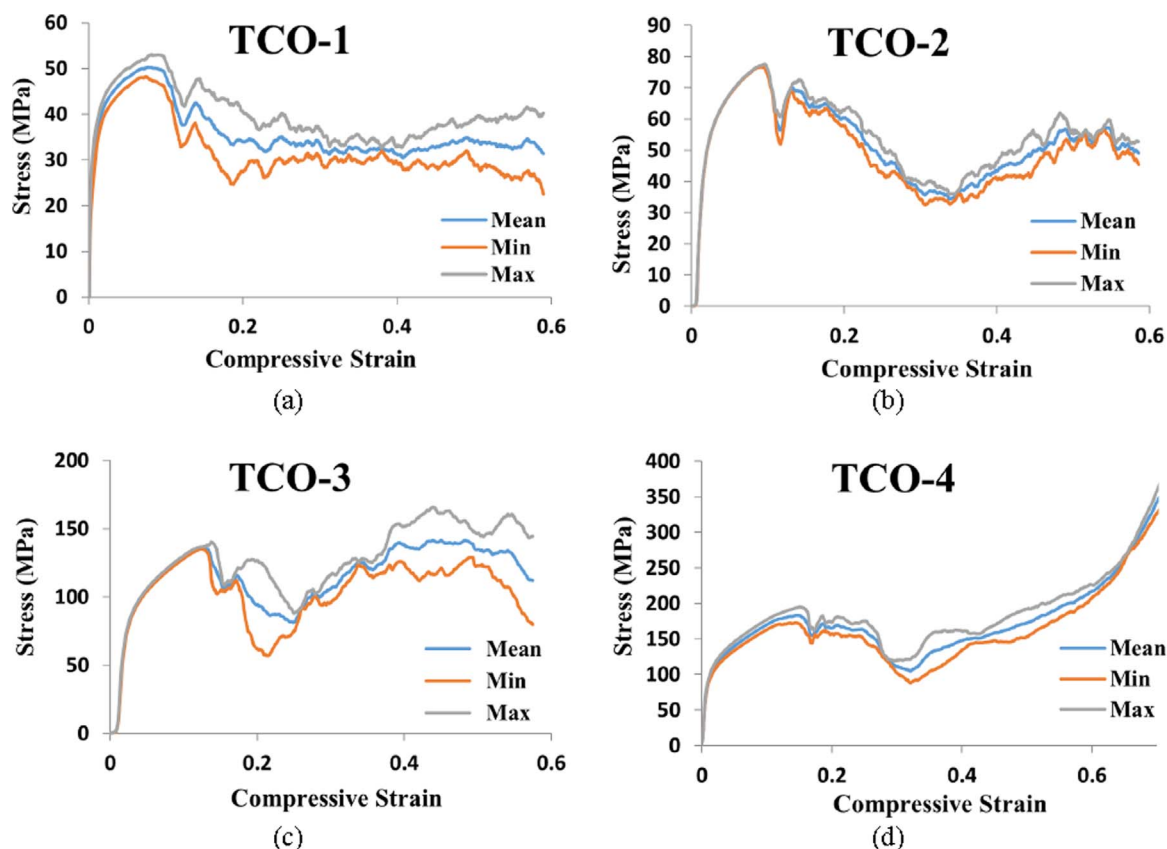


Fig. 6. Stress-strain curves of Co-Cr porous structures based on truncated cuboctahedron unit cell with different relative density values: (a) 0.24, (b) 0.27, (c) 0.34, and (d) 0.39.

the rhombic dodecahedron unit cell (Fig. 9b). For the porous structures based on the diamond and truncated cuboctahedron unit cells, the normalized values of the plateau stress of the Co-Cr structures were higher than those of the Ti-6Al-4V structures (Fig. 9a, c).

The energy absorption capacities of the Co-Cr structures were higher than those of the Ti-6Al-4V structures for the diamond unit cell type, while the opposite held for the rhombic dodecahedron and truncated cuboctahedron unit cells (Fig. 10). The elastic modulus and yield stress vs. relative density curves of commercially pure Ti (CPT, grade 1) porous structures were generally close to those of Ti-6Al-4V structures (Figs. 7 and 8). However, the normalized plateau stress curve of CPT was significantly higher than that of Ti-6Al-4V (Fig. 9).

For all unit cell types, both the Ti-6Al-4V and Co-Cr porous structures showed normalized elastic modulus and normalized yield stress values that were relatively close to the corresponding analytical curves (Figs. 7–10). In the diamond and truncated cuboctahedron unit cells, the normalized elastic modulus curves of both the Ti-6Al-4V and Co-Cr porous structures almost overlapped with the analytical curves (Fig. 7). For the rhombic dodecahedron unit cell, however, the normalized elastic modulus and yield stress of the porous structures made of different materials showed more deviations from each other and from the analytical predictions (Fig. 8).

#### 4. Discussion

The main goal of this study was to find whether the material type, in isolation or in modulation with topology, influences the mechanical properties of AM porous biomaterials. Except a few cases, the normalized elastic modulus and yield stress values of the porous structures made from all the studied materials (Co-Cr, Ti-6Al-4V, and pure titanium) are relatively close to each other and in general agreement with the analytical predictions. The normalized plateau stress and energy absorption capacity of the porous structures made of different

materials, however, showed significant differences with respect to each other (Figs. 9 and 10).

The results of this study clearly show that both topological design and material type are important factors determining the response of AM porous structures although topological design is the dominating factor. It is therefore important to quantify the effects of both factors on the mechanical properties of AM porous biomaterials. The results of this study showed that choosing different materials (and their associated manufacturing parameters) could result in up to 200% difference in the normalized mechanical properties. The results of our previous studies have shown that topological design could cause as much as 1000% differences in the elastic properties (Zadpoor and Hedayati, 2016). Therefore, the topological design is the dominant factor determining the normalized elastic properties of the porous structures.

There could be several reasons behind the relatively minor differences between the normalized elastic modulus and yield stress curves of the porous structures made from different materials. One of the first reasons is the difference between the materials in terms of the AM process including the quality of the powder and suitability of the chosen laser beam parameters such as the laser power and scanning speed. In a study (Murr et al., 2011) which compared the mechanical properties of Co-Cr and Ti-6Al-4V dode-thin porous structures manufactured by electron beam melting (EBM) technique, the relative elastic modulus-relative density diagram of porous structures made from both the materials could be fitted into a single line in a log-log plot. This is in line with our elastic modulus diagram (Fig. 7) which showed that elastic modulus of porous structures made from different materials are all close to each other.

Moreover, compositions and microstructures are important factors influencing the mechanical behavior of AM porous structures. In pure metals, the elastic modulus mainly depends on the inter-atomic forces: metals with smaller inter-atomic distances have higher elastic moduli. As for the metallic alloys, the alloying elements could also change the

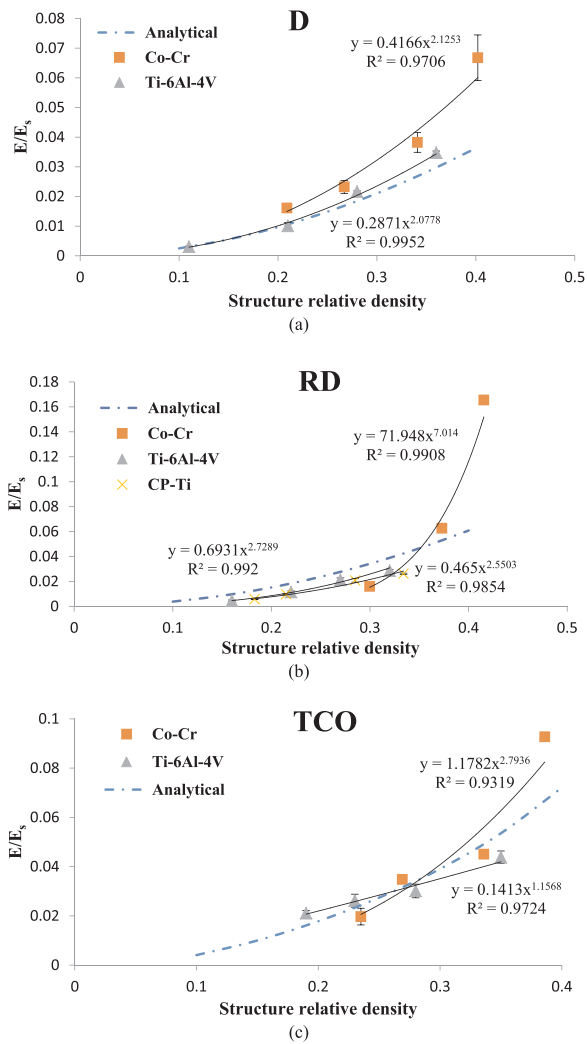


Fig. 7. Comparison of normalized elastic modulus of Ti-6Al-4V, Co-Cr, and CPT porous structures based on (a) diamond, (b) rhombic dodecahedron, and (c) truncated cuboctahedron unit cells.

elastic modulus by introducing lattice distortion or forming second phase particles. Taking Ti-6Al-4V as an example, the  $\alpha$  phase has a higher elastic modulus than the  $\beta$  phase (Fan, 1993; Lee and Welsch, 1990). The elastic modulus of this alloy could therefore vary for different manufacturing processes and different laser processing parameters in AM (Ahmadi et al., 2014), because the compositions of  $\alpha$  and  $\beta$  phases could vary. The same holds for Co-Cr. Although there is no extensive literature describing the effects of different phases on the elastic modulus of AM Co-Cr, the basic phase of Co-Cr is expected to have lower elastic modulus than the second phase in the boundary. In addition to the microstructural compositions, strong crystallographic anisotropy could also cause variations in the elastic modulus, as the elastic modulus is usually dependent on the crystal orientations. These are why the elastic modulus of Ti-6Al-4V could change from 95 GPa to 145 GPa (Vrancken et al., 2012; Facchini et al., 2010; Vilaro et al., 2011) while that of Co-Cr varies between 178 GPa and 230 GPa (Murr et al., 2012; Koutsoukis et al., 2015; España et al., 2010), according to different studies.

It has been shown that the mechanical properties of Co-Cr and Ti-6Al-4V SLM materials in the directions parallel and perpendicular to the building direction can be respectively up to 7% and 10% different (Kajima et al., 2016; Simonelli et al., 2014). While in the analytical derivations, it is assumed that the mechanical properties of the bulk material is constant in all the directions, the experimental data shows

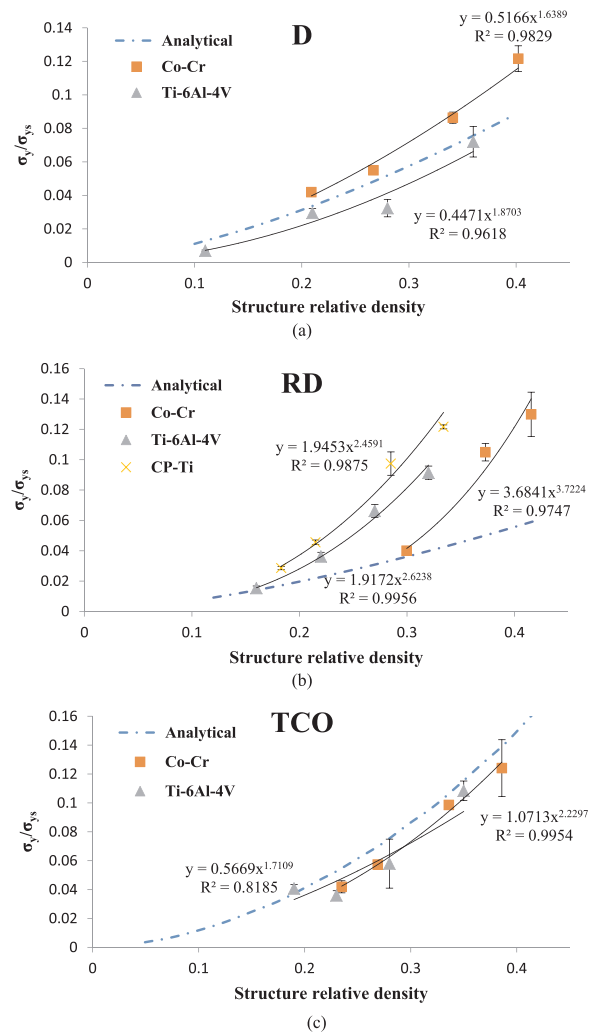


Fig. 8. Comparison of normalized yield stress of Ti-6Al-4V, Co-Cr, and CPT porous structures based on (a) diamond, (b) rhombic dodecahedron, and (c) truncated cuboctahedron unit cells.

difference. The build orientation also affects the porous structures based on different unit cells in different extents, due to the fact that strut orientations are different in different unit cell types.

As for the yield strength, microstructure has a larger contribution. Yield strength is affected by many microstructural characteristics such as grain size, second phase distribution, anisotropy, and cooling rate. Smaller grains lead to more grain boundaries. According to the Hall-Petch relationship, the yield strength of materials increase as the grain size decrease. Smaller grains could decrease the dislocation amount in each dislocation cluster, which decreases the stress concentration. Selective laser melted Co-Cr alloy has a very small columnar grain size, which results in higher yield strengths than conventionally manufactured alloys (Georgette and Davidson, 1986). Moreover, the fine and uniform second phase distributions could improve the yield strength by effectively inhibiting the dislocation movement. SEM pictures of Co-Cr show that the second phases (aligned carbide precipitates (Gaytan et al., 2011)) are all uniformly distributed in the grain boundary (Figure S2b). The pin effect of the second phases in the grain boundary could keep the boundary from sliding. Microstructural anisotropy, textures as well as a number of other parameters could give rise to different yield strengths in different directions. Previous studies have found that yield strength is higher when the (tensile) test direction is perpendicular to the build direction for both selective laser melted Ti-6Al-4V and Co-Cr solid materials (Song et al., 2014; Rafi et al., 2013). Struts in the porous

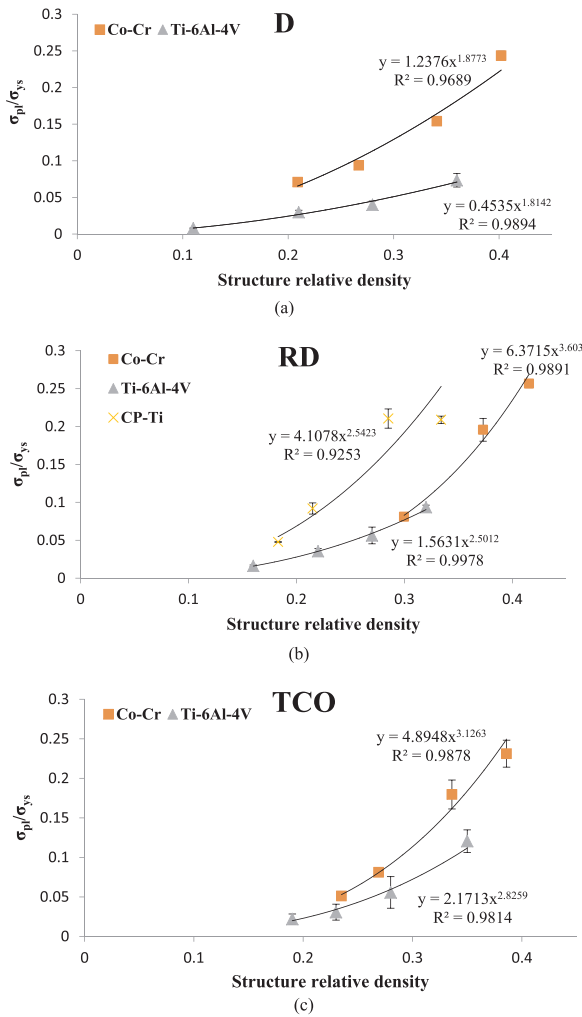


Fig. 9. Comparison of normalized plateau stress of Ti-6Al-4V, Co-Cr, and CPT porous structures based on (a) diamond, (b) rhombic dodecahedron, and (c) truncated octahedron unit cells.

structures are mostly overhang structures, while solid parts are always supported by the former layers. The fully solid parts could therefore generate textures in parallel with the build direction, but the same may not happen in porous materials, as laser has limited influence on the former layer in the tilted struts. Second, rapid cooling of the Ti-6Al-4V during the SLM process creates needle shaped  $\alpha'$  phases in Ti-6Al-4V which increase the strength of the alloy (Ahmed and Rack, 1998). In a similar way, rapid cooling of Co-Cr structures during the SLM process creates finer (Kaiser et al., 2012) more irregular (Murr et al., 2011) columnar dendritic microstructure which increases the yield strength (Zhuang and Langer, 1989). It has been shown that the rapid cooling effect is of greater importance in Ti-6Al-4V as compared to Co-Cr (Murr et al., 2011).

Not all mechanical properties were similar in terms of the effects of topological design and material type. The normalized plateau stress values of pure titanium and Co-Cr were significantly higher than that of Ti-6Al-4V (Fig. 9). Pure titanium and Co-Cr are more ductile and they keep their integrity and (distorted) cell walls up to very large strains, while in the Ti-6Al-4V porous structures, collapsing and crushing of the cells start from the very beginning of deformations. Therefore, in the Ti-6Al-4V porous structures, the stress-strain curves show an initial peak point after yielding followed by considerable fluctuations in the plateau part (see Figs. 4,6 and 7 in (Ahmadi et al., 2015)). After this point, the stress decreases sharply, continuing up to the densification point with stress values much lower than the initial maximum stress. Therefore, in

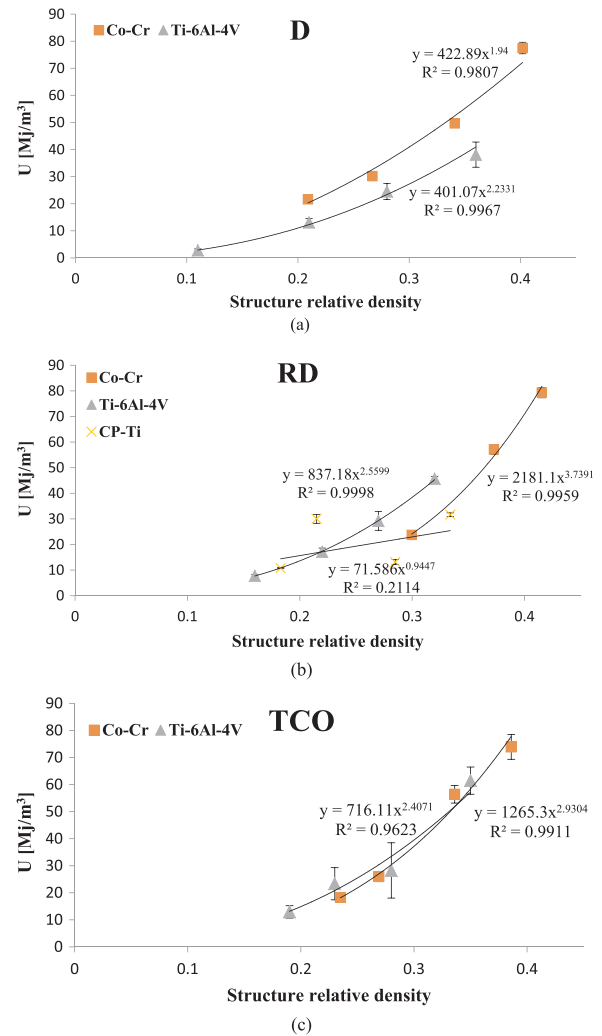


Fig. 10. Comparison of energy absorption of Ti-6Al-4V, Co-Cr, and CPT porous structures based on (a) diamond, (b) rhombic dodecahedron, and (c) truncated octahedron unit cells.

AM porous structures made of Ti-6Al-4V structures, the plateau stress is usually around the yield stress (and much lower than the initial maximum stress) (compare e.g. Figs. 8 and 9). On the other hand, the stress-strain curves of pure titanium do not show any initial peak and stresses keep slowly and constantly accumulate up until the very end of deformations leading to plateau stresses much higher than the yield stress (see Fig. 2a in (Wauthle et al., 2015)). In the stress-strain curves of Co-Cr porous structures, the initial peak point and the fluctuations in the plateau regime are less significant than those in the stress-strain curves of Ti-6Al-4V.

The energy absorption capacity diagrams did not show any particular trend regarding which of the two Co-Cr and Ti-6Al-4V structures could absorb more energy (Fig. 10). The main reason is that the total energy absorption capacity, which was measured up to 60% strain, is a sum of the elastic and plastic energy absorption capacities (respectively represented by elastic modulus and plateau stress) which showed different trends (Figs. 7 and 9).

## 5. Conclusions

This systematic study on the effects of topological design and material type on the mechanical response of AM porous biomaterials showed that topological design has the dominant effect on the normalized elastic modulus and yield stress values. However, the material

properties of the bulk material (such as ductility) could have considerable effects on the plateau stress and energy absorption capacity of the porous structure. Although the effect of material type on the post-elastic response of porous structure is much more significant than its effect on the elastic properties, its effect is still lower as compared to topological design. Quantitatively speaking, topological design could cause up to 10-fold difference in the mechanical properties of AM porous biomaterials while up to 2-fold difference was observed as a consequence of changing the material type.

## Appendix A. Supporting information

Supplementary data associated with this article can be found in the online version at <http://dx.doi.org/10.1016/j.jmbbm.2017.12.029>.

## References

- Ahmadi, S., Campoli, G., Amin Yavari, S., Sajadi, B., Wauthlé, R., Schrooten, J., ... Zadpoor, A.A., 2014. Mechanical behavior of regular open-cell porous biomaterials made of diamond lattice unit cells. *J. Mech. Behav. Biomed. Mater.* 34, 106–115.
- Ahmadi, S., Yavari, S., Wauthle, R., Pouran, B., Schrooten, J., Weinans, H., Zadpoor, A., 2015. Additively manufactured open-cell porous biomaterials made from six different space-filling unit cells: the mechanical and morphological properties. *Materials* 8 (4), 1871–1896.
- Ahmed, T., Rack, H., 1998. Phase transformations during cooling in  $\alpha + \beta$  titanium alloys. *Mater. Sci. Eng.: A* 243 (1), 206–211.
- Amin Yavari, S., Ahmadi, S., Wauthle, R., Pouran, B., Schrooten, J., Weinans, H., Zadpoor, A., 2015. Relationship between unit cell type and porosity and the fatigue behavior of selective laser melted meta-biomaterials. *J. Mech. Behav. Biomed. Mater.* 43, 91–100.
- Amin Yavari, S., Loozen, L., Paganelli, F.L., Bakshandeh, S., Lietaert, K., Groot, J.A., ... Vogely, H.C., 2016. Antibacterial behavior of additively manufactured porous titanium with nanotubular surfaces releasing silver ions. *ACS Appl. Mater. Interfaces* 8 (27), 17080–17089.
- Babaei, S., Jahromi, B.H., Ajdari, A., Nayeb-Hashemi, H., Vaziri, A., 2012. Mechanical properties of open-cell rhombic dodecahedron cellular structures. *Acta Materialia* 60 (6), 2873–2885.
- Bandyopadhyay, A., Bose, S., 2016. *Bone Replacement Materials: Google Patents*.
- Bandyopadhyay, A., Espana, F., Balla, V.K., Bose, S., Ohgami, Y., Davies, N.M., 2010. Influence of porosity on mechanical properties and in vivo response of Ti6Al4V implants. *Acta Biomater.* 6 (4), 1640–1648.
- Bandyopadhyay, A., Krishna, B., Xue, W., Bose, S., 2009. Application of laser engineered net shaping (LENS) to manufacture porous and functionally graded structures for load bearing implants. *J. Mater. Sci.: Mater. Med.* 20 (1), 29.
- España, F.A., Balla, V.K., Bose, S., Bandyopadhyay, A., 2010. Design and fabrication of CoCrMo alloy based novel structures for load bearing implants using laser engineered net shaping. *Mater. Sci. Eng.: C* 30 (1), 50–57. <http://dx.doi.org/10.1016/j.msec.2009.08.006>.
- Facchini, L., Magalini, E., Robotti, P., Molinari, A., Höges, S., Wissenbach, K., 2010. Ductility of a Ti-6Al-4V alloy produced by selective laser melting of prealloyed powders. *Rapid Prototyp. J.* 16 (6), 450–459. <http://dx.doi.org/10.1108/13552541011083371>.
- Fan, Z., 1993. On the Young's moduli of Ti-6Al-4V alloys. *Scr. Metall. Mater.* 29 (11), 1427–1432. [http://dx.doi.org/10.1016/0956-716X\(93\)90331-L](http://dx.doi.org/10.1016/0956-716X(93)90331-L).
- Gaytan, S.M., Murr, L.E., Ramirez, D.A., Machado, B.I., Martinez, E., Hernandez, D.H., ... Wicker, R.B., 2011. A TEM study of cobalt-base alloy prototypes fabricated by EBM. *Mater. Sci. Appl.* 2 (05), 355.
- Georgette, F., Davidson, J., 1986. The effect of HIPing on the fatigue and tensile strength of a cast, porous-coated Co-Cr-Mo alloy. *J. Biomed. Mater. Res. Part A* 20 (8), 1229–1248.
- Gibson, L.J., Ashby, M.F., 1999. *Cellular Solids: Structure and Properties*. Cambridge University Press.
- Han, C., Han, C., Yan, C., Yan, C., Wen, S., Wen, S., ... Li, S., 2017. Effects of the unit cell topology on the compression properties of porous Co-Cr scaffolds fabricated via selective laser melting. *Rapid Prototyp. J.* 23 (1), 16–27.
- Hedayati, R., Hosseini-Toudeshky, H., Sadighi, M., Mohammadi-Aghdam, M., Zadpoor, A., 2016. Computational prediction of the fatigue behavior of additively manufactured porous metallic biomaterials. *Int. J. Fatigue* 84, 67–79.
- Hedayati, R., Sadighi, M., Mohammadi-Aghdam, M., Zadpoor, A., 2016a. Mechanical behavior of additively manufactured porous biomaterials made from truncated cuboctahedron unit cells. *Int. J. Mech. Sci.* 106, 19–38.
- Hedayati, R., Sadighi, M., Mohammadi-Aghdam, M., Zadpoor, A.A., 2016b. Mechanical properties of regular porous biomaterials made from truncated cube repeating unit cells: analytical solutions and computational models. *Mater. Sci. Eng.: C* 60, 163–183.
- Hedayati, R., Sadighi, M., Mohammadi-Aghdam, M., Zadpoor, A.A., 2016c. Mechanics of additively manufactured porous biomaterials based on the rhombicuboctahedron unit cell. *J. Mech. Behav. Biomed. Mater.* 53, 272–294.
- Heritage, K., Frisby, C., Wolfenden, A., 1988. Impulse excitation technique for dynamic flexural measurements at moderate temperature. *Rev. Sci. Instrum.* 59 (6), 973–974.
- Hollister, S.J., 2005. Porous scaffold design for tissue engineering. *Nat. Mater.* 4 (7), 518–524.
- Hollister, S.J., Maddox, R., Taboas, J.M., 2002. Optimal design and fabrication of scaffolds to mimic tissue properties and satisfy biological constraints. *Biomaterials* 23 (20), 4095–4103.
- Hutmacher, D.W., 2000. Scaffolds in tissue engineering bone and cartilage. *Biomaterials* 21 (24), 2529–2543.
- Jia, Z., Xiu, P., Xiong, P., Zhou, W., Cheng, Y., Wei, S., ... Liu, Z., 2016. Additively manufactured macroporous titanium with silver-releasing micro/nanoporous surface for multipurpose infection control and bone repair – a proof of concept. *ACS Appl. Mater. Interfaces*.
- Kaiser, R., Browne, D., Williamson, K., 2012. Investigation of the effects of cooling rate on the microstructure of investment cast biomedical grade Co alloys. Paper Presented at the IOP Conference Series: Materials Science and Engineering.
- Kajima, Y., Takaichi, A., Nakamoto, T., Kimura, T., Yogo, Y., Ashida, M., ... Hanawa, T., 2016. Fatigue strength of Co–Cr–Mo alloy clasps prepared by selective laser melting. *J. Mech. Behav. Biomed. Mater.* 59, 446–458.
- Kalidindi, S., Abusafieh, A., El-Danaf, E., 1997. Accurate characterization of machine compliance for simple compression testing. *Exp. Mech.* 37 (2), 210–215.
- Ko, W., 1965. Deformations of foamed elastomers. *J. Cell. Plast.* 1 (1), 45–50.
- Koutsoukis, T., Zinelis, S., Eliades, G., Al-Wazzan, K., Rifaiy, M.A., Al Jabbari, Y.S., 2015. Selective laser melting technique of Co-Cr dental alloys: a review of structure and properties and comparative analysis with other available techniques. *J. Prosthodont.* 24 (4), 303–312.
- Krishna, B.V., Bose, S., Bandyopadhyay, A., 2007. Low stiffness porous Ti structures for load-bearing implants. *Acta Biomater.* 3 (6), 997–1006.
- Krishna, B.V., Xue, W., Bose, S., Bandyopadhyay, A., 2008. Engineered porous metals for implants. *JOM* 60 (5), 45–48.
- Lee, Y.T., Welsch, G., 1990. Young's modulus and damping of Ti-6Al-4V alloy as a function of heat treatment and oxygen concentration. *Mater. Sci. Eng.: A* 128 (1), 77–89. [http://dx.doi.org/10.1016/0921-5093\(90\)90097-M](http://dx.doi.org/10.1016/0921-5093(90)90097-M).
- Li, S., Xu, Q., Wang, Z., Hou, W., Hao, Y., Yang, R., Murr, L., 2014. Influence of cell shape on mechanical properties of Ti-6Al-4V meshes fabricated by electron beam melting method. *Acta Biomater.* 10 (10), 4537–4547.
- Lin, C.Y., Kikuchi, N., Hollister, S.J., 2004. A novel method for biomaterial scaffold internal architecture design to match bone elastic properties with desired porosity. *J. Biomech.* 37 (5), 623–636.
- Liu, X., Wu, S., Yeung, K.W., Chan, Y., Hu, T., Xu, Z., ... Chu, P.K., 2011. Relationship between osseointegration and superelastic biomechanics in porous NiTi scaffolds. *Biomaterials* 32 (2), 330–338.
- Murr, L., Amato, K., Li, S., Tian, Y., Cheng, X., Gaytan, S., ... Wicker, R., 2011. Microstructure and mechanical properties of open-cellular biomaterials prototypes for total knee replacement implants fabricated by electron beam melting. *J. Mech. Behav. Biomed. Mater.* 4 (7), 1396–1411.
- Murr, L., Li, S., Tian, Y., Amato, K., Martinez, E., Medina, F., 2011. Open-cellular Co-base and Ni-base superalloys fabricated by electron beam melting. *Materials* 4 (4), 782–790.
- Murr, L.E., Gaytan, S.M., Martinez, E., Medina, F., Wicker, R.B., 2012. Next generation orthopaedic implants by additive manufacturing using electron beam melting. *Int. J. Biomater.* 2012, 14. <http://dx.doi.org/10.1155/2012/245727>.
- Pattanayak, D.K., Fukuda, A., Matsushita, T., Takemoto, M., Fujibayashi, S., Sasaki, K., ... Kokubo, T., 2011. Bioactive Ti metal analogous to human cancellous bone: fabrication by selective laser melting and chemical treatments. *Acta Biomater.* 7 (3), 1398–1406.
- Ptochos, E., Labeas, G., 2012. Elastic modulus and Poisson's ratio determination of micro-lattice cellular structures by analytical, numerical and homogenisation methods. *J. Sandw. Struct. Mater.* 1099636212444285.
- Pyka, G., Burakowski, A., Kerckhofs, G., Moesen, M., Van Bael, S., Schrooten, J., Wevers, M., 2012. Surface modification of Ti6Al4V open porous structures produced by additive manufacturing. *Adv. Eng. Mater.* 14 (6), 363–370.
- Rafi, H.K., Starr, T.L., Stucker, B.E., 2013. A comparison of the tensile, fatigue, and fracture behavior of Ti-6Al-4V and 15-5 PH stainless steel parts made by selective laser melting. *Int. J. Adv. Manuf. Technol.* 69 (5), 1299–1309. <http://dx.doi.org/10.1007/s00170-013-5106-7>.
- Simonelli, M., Tse, Y.Y., Tuck, C., 2014. Effect of the build orientation on the mechanical properties and fracture modes of SLM Ti-6Al-4V. *Mater. Sci. Eng.: A* 616, 1–11.
- Song, C., Yang, Y., Wang, Y., Wang, D., Yu, J., 2014. Research on rapid manufacturing of CoCrMo alloy femoral component based on selective laser melting. *Int. J. Adv. Manuf. Technol.* 75 (1), 445–453. <http://dx.doi.org/10.1007/s00170-014-6150-7>.
- Staiger, M.P., Pietak, A.M., Huadmai, J., Dias, G., 2006. Magnesium and its alloys as orthopedic biomaterials: a review. *Biomaterials* 27 (9), 1728–1734.
- Standard I. ISO 13314: 2011 (E), 2011. *Mechanical Testing of Metals—Ductility Testing—Compression Test for Porous and Cellular Metals. Ref Number ISO 13314(13314)*, pp. 1–7.
- Vaithilingam, J., Kilsby, S., Goodridge, R.D., Christie, S.D., Edmondson, S., Hague, R.J., 2014. Immobilisation of an antibacterial drug to Ti6Al4V components fabricated using selective laser melting. *Appl. Surf. Sci.* 314, 642–654.
- Van Bael, S., Chai, Y.C., Truscetto, S., Moesen, M., Kerckhofs, G., Van Oosterwyck, H., Schrooten, J., 2012. The effect of pore geometry on the in vitro biological behavior of human periosteum-derived cells seeded on selective laser-melted Ti6Al4V bone scaffolds. *Acta Biomater.* 8 (7), 2824–2834.
- Van Hooreweder, B., Apers, Y., Lietaert, K., Kruth, J.-P., 2017. Improving the fatigue performance of porous metallic biomaterials produced by Selective Laser Melting. *Acta Biomater.* 47, 193–202.
- Vilaro, T., Colin, C., Bartout, J.D., 2011. As-fabricated and heat-treated microstructures of the Ti-6Al-4V alloy processed by selective laser melting. *Mettall. Mater. Trans. A* 42 (10), 3190–3199. <http://dx.doi.org/10.1007/s11661-011-0731-y>.
- Vrancken, B., Thijs, L., Kruth, J.-P., Van Humbeeck, J., 2012. Heat treatment of Ti6Al4V

- produced by selective laser melting: microstructure and mechanical properties. *J. Alloy. Compd.* 541, 177–185.
- Wang, X., Xu, S., Zhou, S., Xu, W., Leary, M., Choong, P., ... Xie, Y.M., 2016. Topological design and additive manufacturing of porous metals for bone scaffolds and orthopaedic implants: a review. *Biomaterials* 83, 127–141.
- Warren, W., Kraynik, A., 1997. Linear elastic behavior of a low-density Kelvin foam with open cells. *J. Appl. Mech.* 64 (4), 787–794.
- Wauthle, R., Ahmadi, S.M., Yavari, S.A., Mulier, M., Zadpoor, A.A., Weinans, H., ... Schrooten, J., 2015. Revival of pure titanium for dynamically loaded porous implants using additive manufacturing. *Mater. Sci. Eng.: C* 54, 94–100.
- Yavari, S.A., Wauthlé, R., Böttger, A.J., Schrooten, J., Weinans, H., Zadpoor, A.A., 2014. Crystal structure and nanotopographical features on the surface of heat-treated and anodized porous titanium biomaterials produced using selective laser melting. *Appl. Surf. Sci.* 290, 287–294.
- Zadpoor, A.A., 2015. Bone tissue regeneration: the role of scaffold geometry. *Biomater. Sci.* 3 (2), 231–245.
- Zadpoor, A.A., Hedayati, R., 2016. Analytical relationships for prediction of the mechanical properties of additively manufactured porous biomaterials. *J. Biomed. Mater. Res. Part A* 104 (12), 3164–3174.
- Zheng, X., Lee, H., Weisgraber, T.H., Shusteff, M., DeOtte, J., Duoss, E.B., ... Jackson, J.A., 2014. Ultralight, ultrastiff mechanical metamaterials. *Science* 344 (6190), 1373–1377.
- Zhu, H., Knott, J., Mills, N., 1997. Analysis of the elastic properties of open-cell foams with tetrakaidecahedral cells. *J. Mech. Phys. Solids* 45 (3), 3193–3253.
- Zhuang, L., Langer, E., 1989. Effects of cooling rate control during the solidification process on the microstructure and mechanical properties of cast Co-Cr-Mo alloy used for surgical implants. *J. Mater. Sci.* 24 (2), 381–388.